ADVANCED MATERIALS

Supporting Information

for *Adv. Mater.*, DOI: 10.1002/adma.201703343

Water-Rich Biomimetic Composites with Abiotic Self-Organizing Nanofiber Network

*Lizhi Xu, Xueli Zhao, Chuanlai Xu, and Nicholas A. Kotov**

Supporting Information

Water-Rich Biomimetic Composites with Abiotic Self-Organizing Nanofiber Network

*Lizhi Xu, Xueli Zhao, Chuanlai Xu and Nicholas A. Kotov**

The Supporting Information includes:

Figures S1-S17

Table S1

References [37-44]

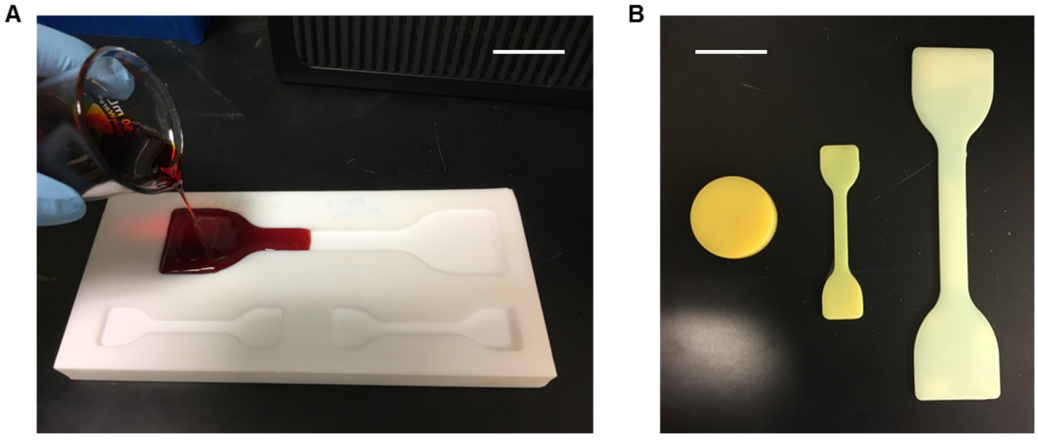

Figure S1. Photographs of the molding process (**A**) and ANF-PVA composite hydrogel samples with various shapes (**B**) made therefrom.

Scale bars: 5 cm.

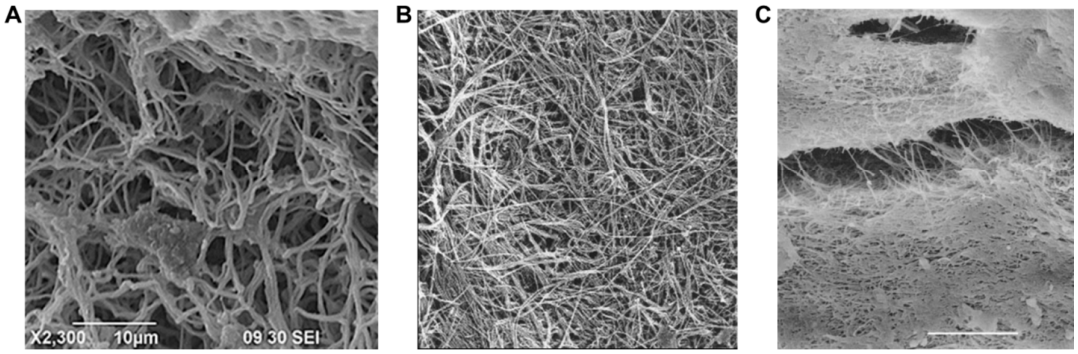

Figure S2. SEM images of collagen nanofiber networks in biological connective tissues. (**A**) cornea. Reproduced from reference [37]. (**B**-**C**) Articulate cartilage. Reproduced from reference [38] (**B**), and [39] (**C**). Scale bar: 3 µm (**C**).

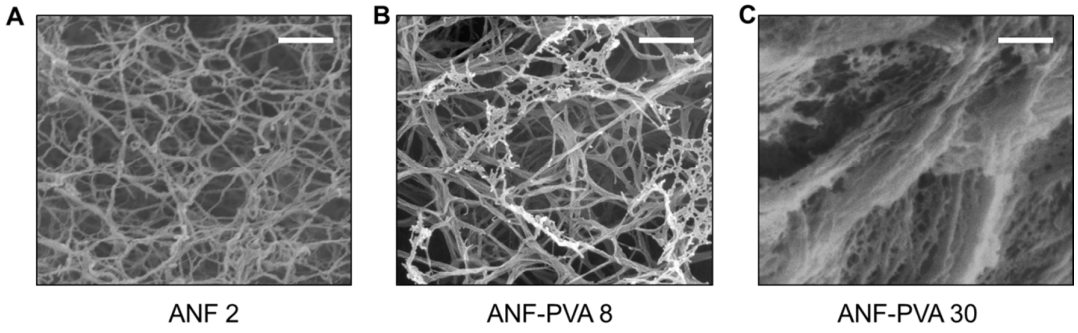

Figure S3. SEM images of ANF 2 (**A**), ANF-PVA 8 (**B**), and ANF-PVA 30 (**C**).

Scale bars: 500 nm.

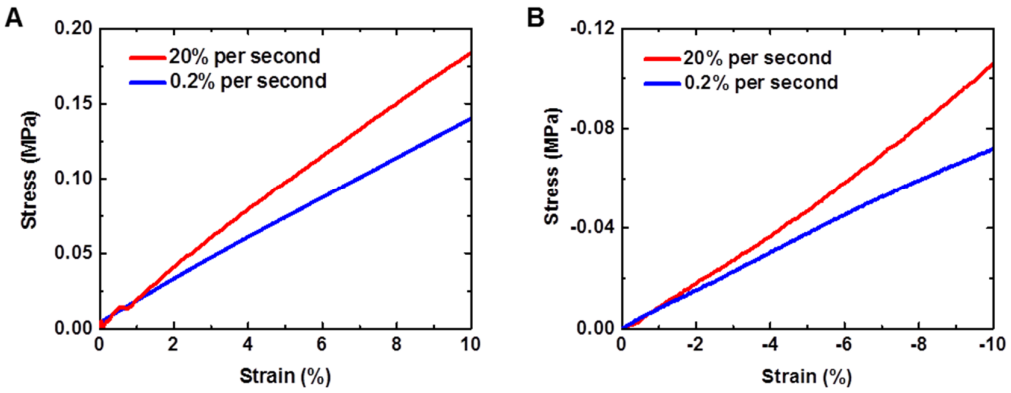

Figure S4. Effect of strain rate on the stiffness of ANF-PVA hydrogels.

Higher strain rates result in greater stiffness of ANF-PVA 8 hydrogels, as characterized by tensile (**A**) or compressive (**B**) tests.

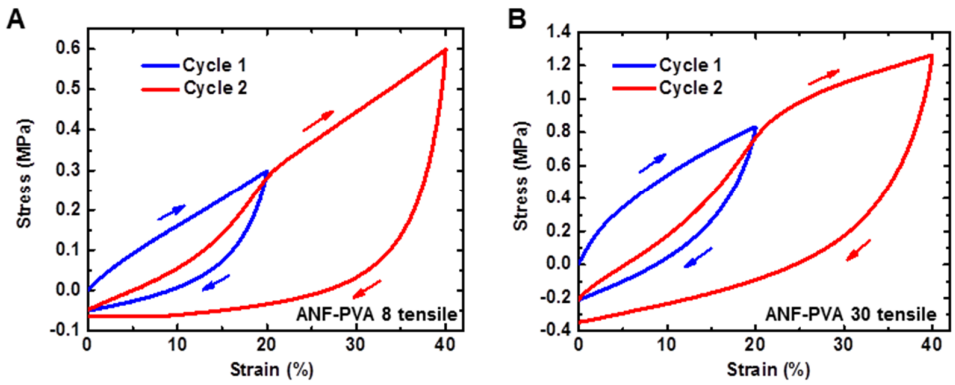

Figure S5. Mullins' effect in ANF-PVA composite hydrogels.

Cyclic tensile tests reveal that the stress-strain curve is dependent on the maximum loading that the material encountered previously. Such behavior is also characteristic of filled rubber and soft tissues and is associated with viscoelasticity as well as the toughness of the materials [40].

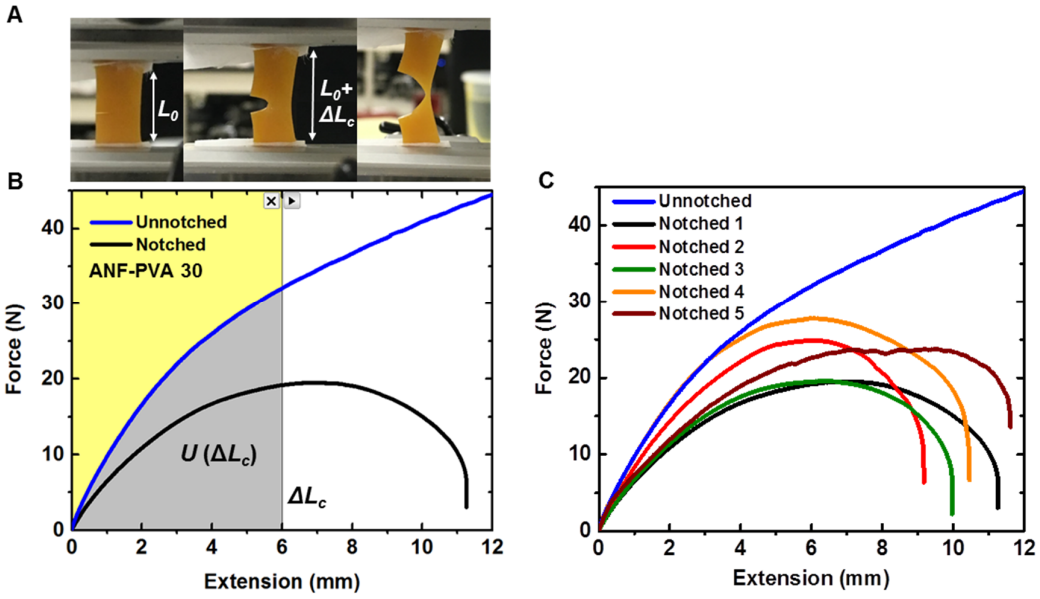

Figure S6. Fracture energy of ANF-PVA 30.

The method for determining fracture energy of hydrogels is described in reference [10]. Briefly, a notch is introduced by a razor blade cutting into a tensile test sample, with A as the area of cross section of the unnotched sample and L_0 as the initial distance between the clamps. The dimension of the samples is not critical for determination of the fracture energy. The length of the notch is approximately halfway across the sample but is likewise not critical. A force-extension curve is measured for both the notched sample and an unnotched sample with the same initial dimensions. ΔL_c is defined as the critical extension where the notch turns into a running crack, and $U(\Delta L_c)$ is the work done to an unnotched sample to reach ΔL_c extension (calculated as the integral of the force-extension curve). The fracture energy is given by: $\Gamma = U(\Delta L_c)/A$. For ANF-PVA 30, a fracture energy of 9,200±2,200 J/m^2 was obtained from measurements on five notched samples, with A=12 mm^2 and L_0=13 mm.

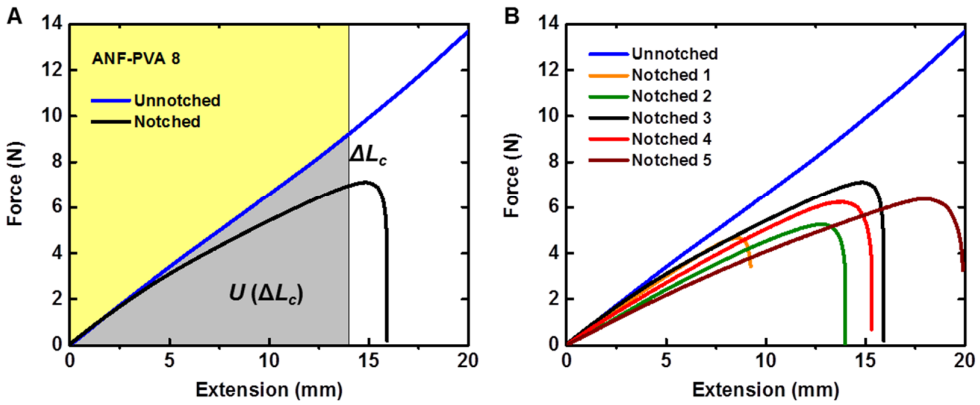

Figure S7. Fracture energy of ANF-PVA 8.

Γ=2,300±1,100 J/m^2 was obtained from measurements on five notched samples of ANF-PVA 8, with A=25 mm^2 and L_0=80 mm.

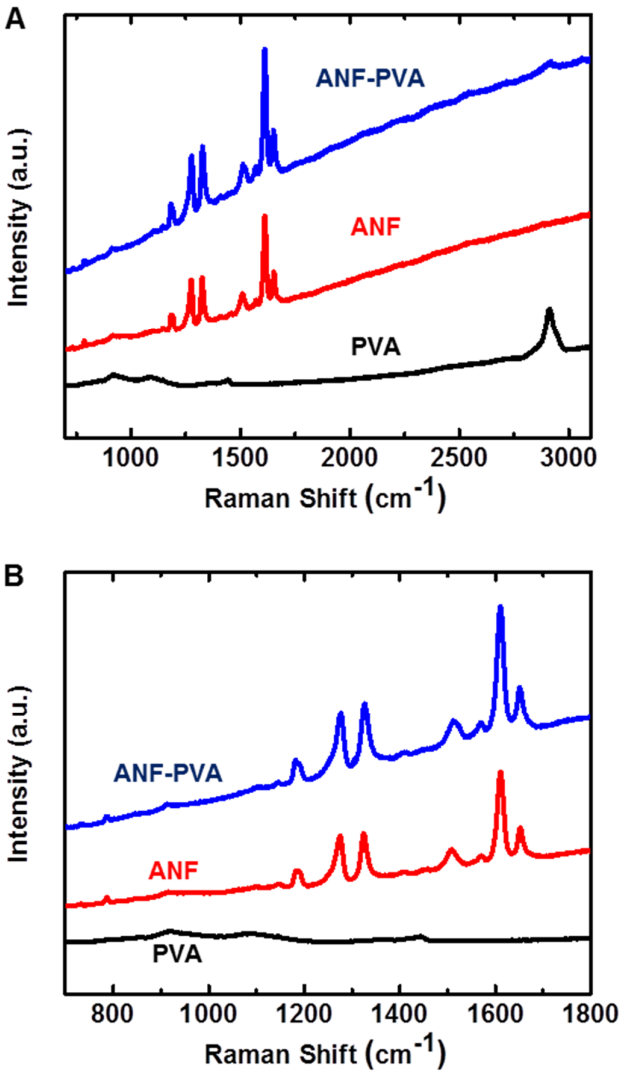

Figure S8. Raman scattering spectroscopy of ANF-PVA, ANF and PVA.

The peaks of the ANF-PVA spectra appear to be additive from ANF and PVA, validating the absence of covalent bonding between the two components.

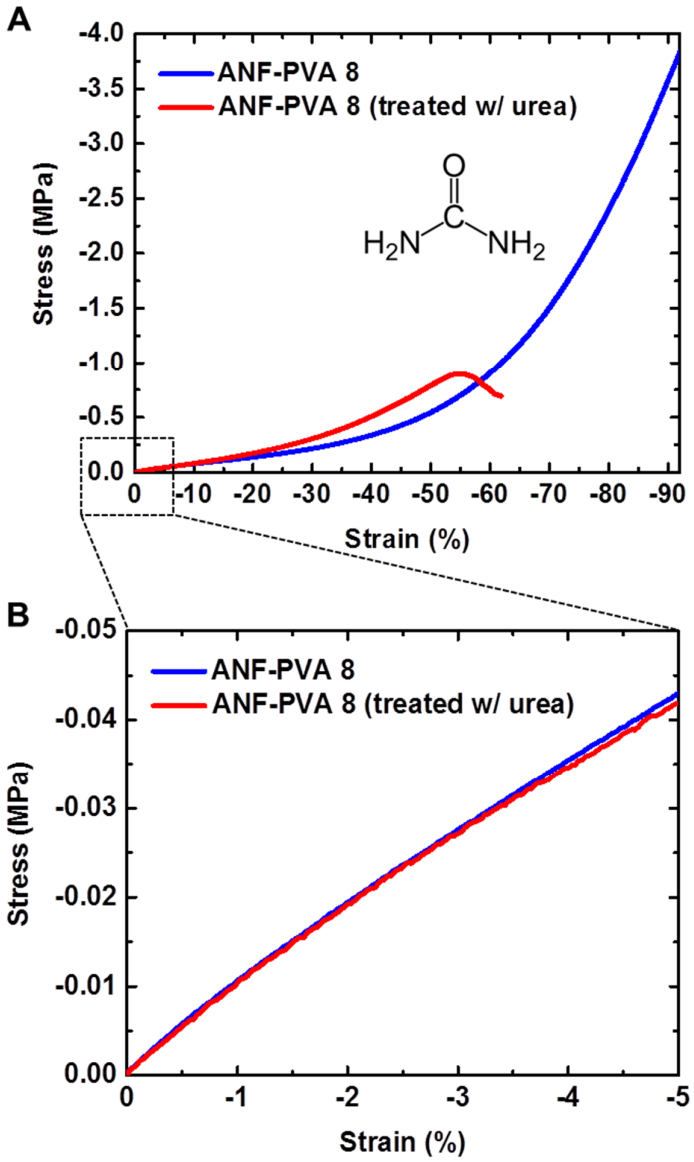

Figure S9. Effect of urea treatment on the mechanical properties of ANF-PVA hydrogels. ANF-PVA 8 hydrogels were soaked in 5 M aqueous solution of urea and heated at 100 ^{o}C for 8 hours. After the treatment, the samples were rinsed with deionized (DI) water and soaked in DI water for 8 hours. Compression tests reveal the significantly reduced mechanical strength of the urea-treated samples.

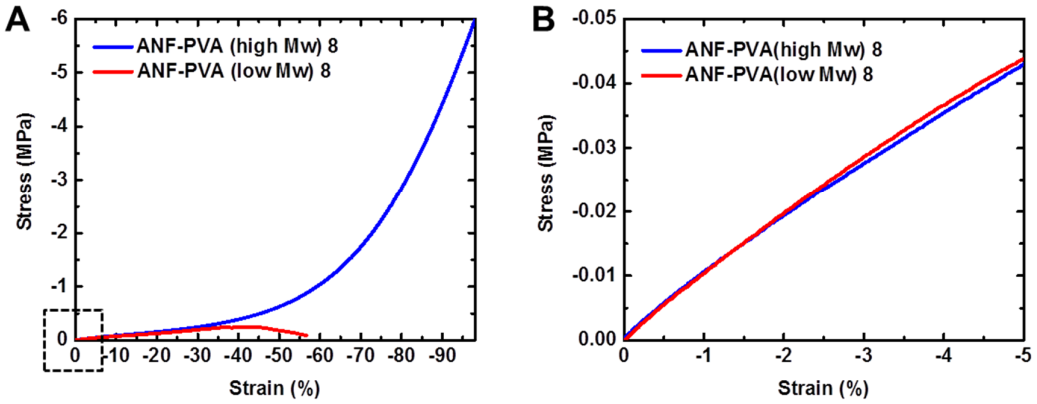

Figure S10. Effects of molecular weight (Mw) of PVA on the mechanical properties of ANF-PVA composite hydrogels.

Compression tests reveal the drastically different mechanical strengths of ANF-PVA 8 hydrogels prepared using PVA samples with Mw values of 13,000-23,000 a.u. (low Mw) or 146,000-186,000 a.u. (high Mw), respectively.

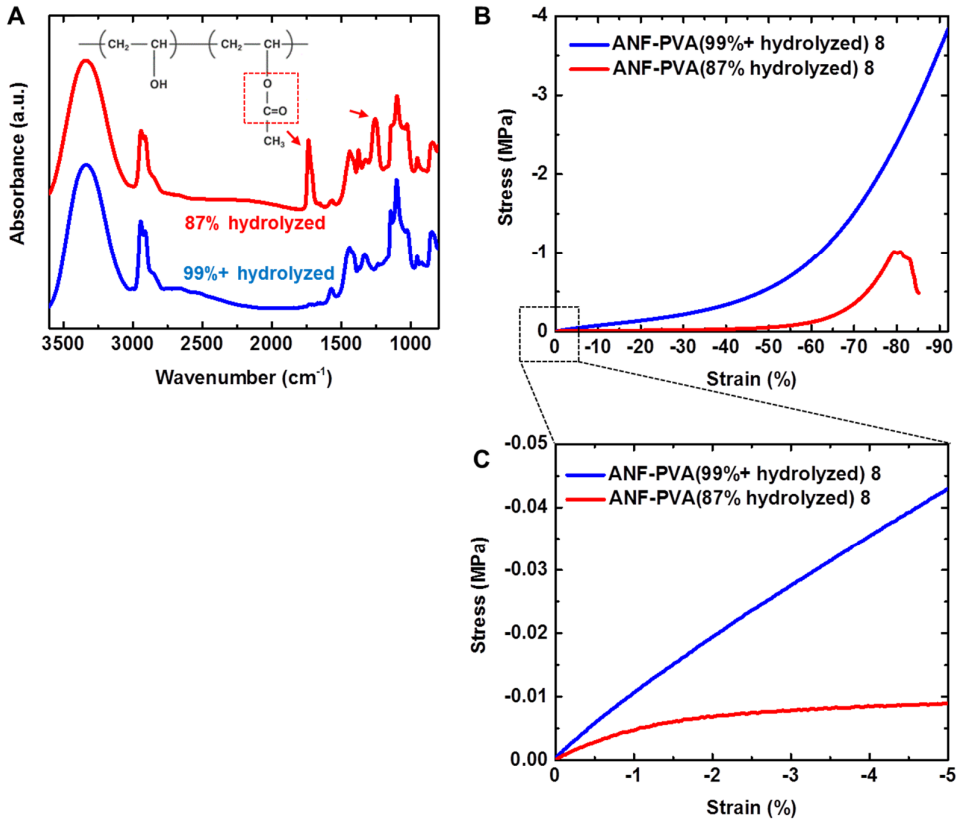

Figure S11. Degree of hydrolysis of PVA and its effects on the mechanical properties of ANF-PVA composite hydrogels.

(**A**) FTIR spectra of 87% and 99%+ hydrolyzed PVA, respectively. The acetate group in the PVA sample with a lower degree of hydrolysis can be characterized by the acetate C=O and C-O stretching bands that are absent in spectra from highly hydrolyzed PVA. (**B-C**) Compression tests on ANF-PVA 8 hydrogels with different degrees of hydrolysis of PVA components. Samples with 87% hydrolyzed PVA show dramatically lower modulus and strength than those with 99%+ hydrolyzed PVA, despite the fact that they have the same weight fraction of the solid content (~8%).

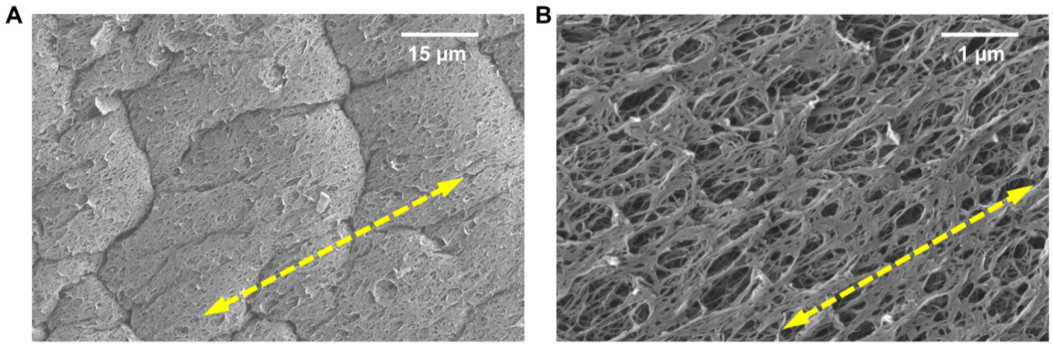

Figure S12. SEM images of the surface of a relaxed ANF-PVA 8 sample after one loading-unloading cycle of 60% tensile strain.

Stress-induced crimping (**A**) and alignment (**B**) can be seen in the nanofibrous composite network. The yellow arrow indicates the direction of tension.

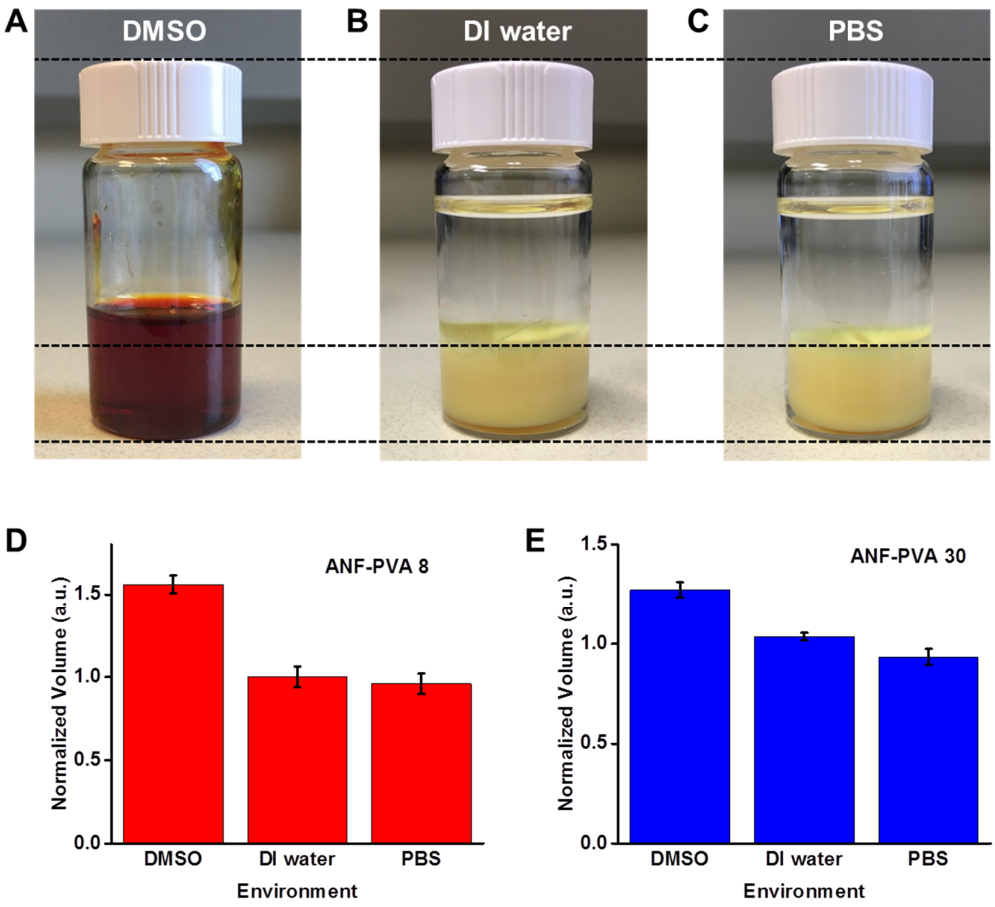

Figure S13. "Non-swelling" behaviors of ANF-PVA hydrogels in aqueous environment. (**A**-**C**) Photographs of an ANF-PVA 8 sample with DMSO before solvent exchange (**A**), 3 days after solvent exchange with deionized (DI) water (**B**), and after immersing in phosphate buffered saline (PBS) at 37 °C for 7 days (**C**). (**D**, **E**) Measurements on volumes of ANF-PVA 8 samples (**D**) and ANF-PVA 30 samples (**E**) in various solvent environments, indicating that they experience a slight shrinkage through DMSO-water exchange, and exhibit little changes in volume when DI water is replaced by PBS at 37 °C.

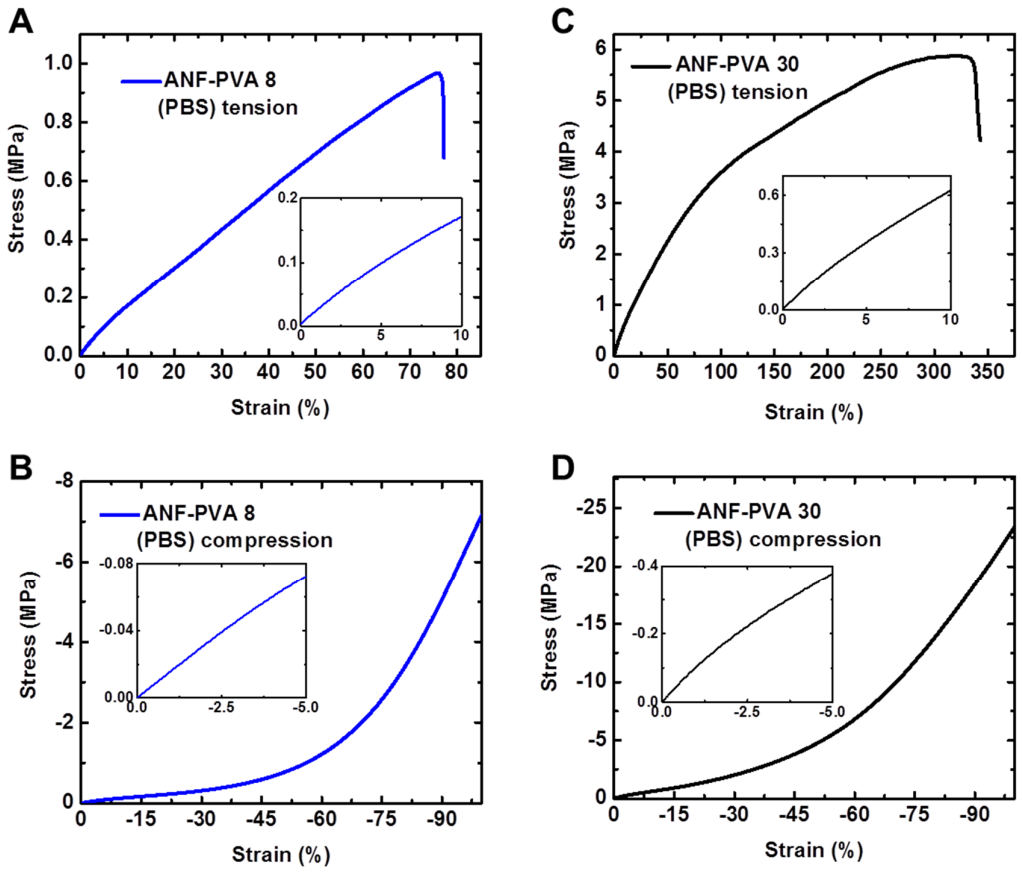

Figure S14. Mechanical characteristics of ANF-PVA hydrogels with treatment in PBS environment.

Samples of ANF-PVA 8 (**A**, **B**) and ANF-PVA 30 (**C**, **D**) were immersed in PBS at 37 °C for 7 days and immediately characterized by tensile (**A**, **C**) or compressive (**B**, **D**) tests after taking out of the PBS bath. They exhibit nearly identical mechanical characteristics to the standard samples prepared with DI water (**Figure 2**).

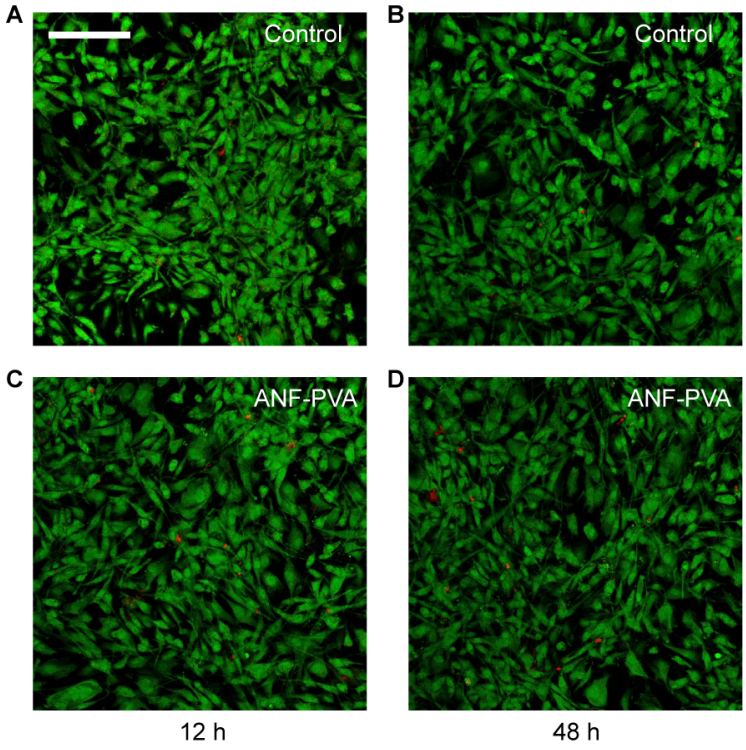

Figure S15. Confocal fluorescence microscopy images of human cartilage cells cultured on ANF-PVA 8 composite hydrogels (**A**, **B**) or on Petri dish (**C**, **D**) for 12 hours (**A**, **C**) and 48 hours (**B**, **D**), respectively.

Live cell fluoresce in green. Dead cell fluoresce in red. Scale bar: 150 μm.

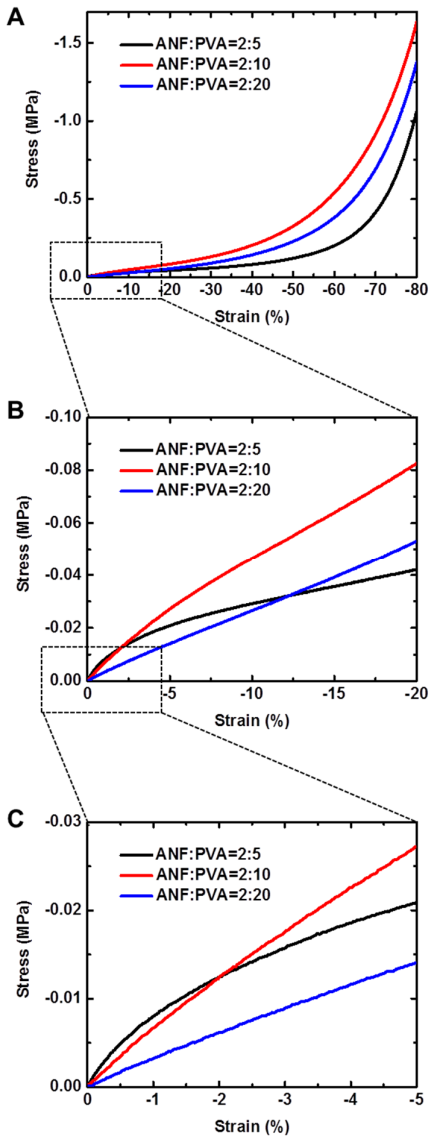

Figure S16. Effects of the ANF/PVA mixing ratio on the mechanical properties of composite hydrogels.

Compression tests characterize the different mechanical behaviors resulting from different mixing ratios. The weight fraction of the solid content was fixed at ~6% for all the samples. The optimal ANF:PVA ratio was found to be 2:10, as evidenced by both high modulus and high strength.

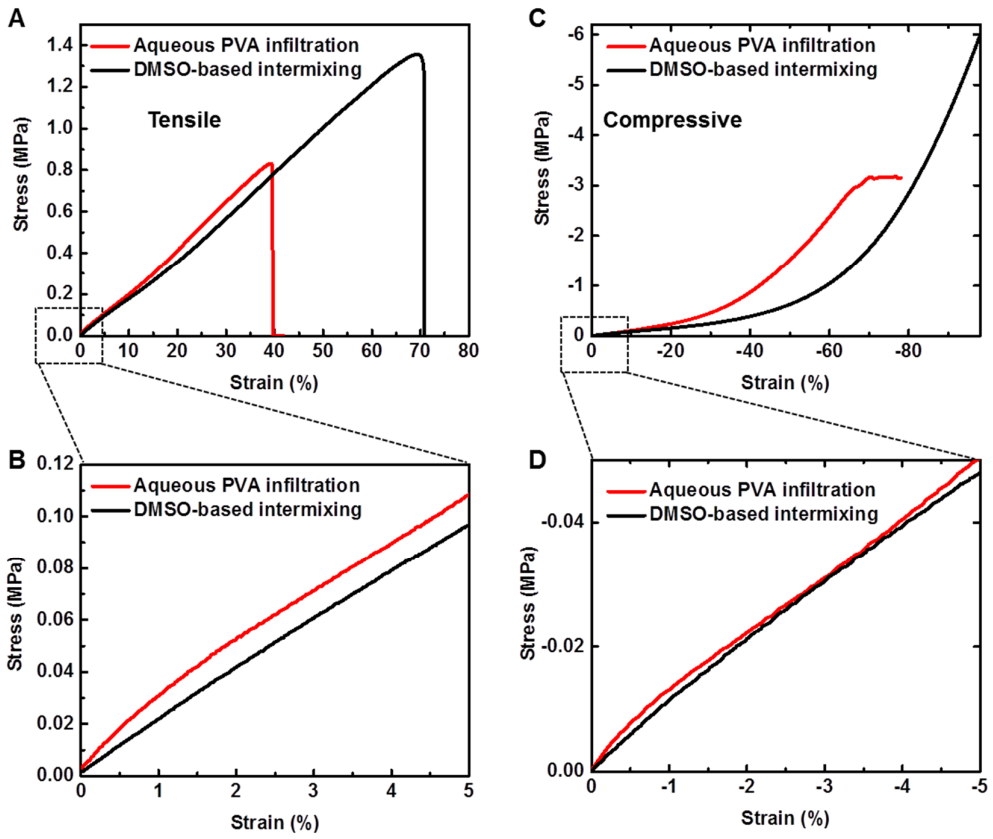

Figure S17. Effects of different preparation methods on the mechanical properties of the composite hydrogels.

The samples based on aqueous PVA infiltration were prepared by soaking 5mm-thick pieces of ANF 2 in 5 wt% aqueous PVA solution at 80 ^{o}C for 7 days. The samples were then rinsed and soaked in DI water for 12 hours. Regular ANF-PVA 8 samples prepared by DMSO-based intermixing and subsequent solvent exchange were tested for comparison. The weight fraction of solid content was ~8% for both types of samples. Although they led to similar tensile and compressive moduli, aqueous PVA infiltration results in samples with dramatically lower mechanical strengths than samples prepared by DMSO-based processes.

Table S1. Comparison of the physical properties of ANF-PVA hydrogels with other representative fiber-reinforced hydrogels.

We note that typical fiber-reinforcement strategies for hydrogels do not result in sets of properties comparable to those of ANF-PVA composites. The unique combination of metrics of ANF-PVA can be attributed to the distinct self-assembled nanofiber network, as well as the reconfigurable, non-covalent interactions at nanomaterial interfaces.

Fiber Type	Reference	Water Content (wt%)	Tensile Modulus (MPa)	Tensile Strength (MPa)	Failure Tensile Strain (%)	Compressive Modulus (MPa)	Compressive Strength (MPa)	Failure Compressive Strain (%)
ANF-PVA	**Present Work**	**92-70**	**1.9-9.1**	**1.4-5.0**	**70-325**	**1.0-4.0**	**5.9-26.5**	**>99**
Nano-Crystalline Cellulose	[15]	85	~1	~1	~100			
Bacterial Cellulose	[14]	91-68	5-2[a)]	1.1-3.8[a)]	22-28[a)]	1.3-3.9[a)]	2.1-5.3[a)]	31-44[a)]
Carbon Nanotube	[41]		0.01-0.06	0.05-0.25	150-250	0.01-0.03	0.1	50-70
Electrospun Polymeric Nanofibers	[42]	~90	0.2-0.6	0.02-0.35	15-180	0.01-0.02	0.03-0.07	52-66
Woven Textile	[43, 44]	75-40	0.8-3.7	0.08-2.1	10-247	0.1-0.2		

a) Anisotropic (highest values are shown)

References:

[37] W. F. Abdallah, S. G. Louie, Y. Zhang, K. E. Rodgers, E. Sivok, G. S. Dizerega, M. S. Humayun, *Investig. Ophthalmol. Vis. Sci.* **2016**, *57*, 2187.
[38] D. W. Goodwin, H. Zhu, J. F. Dunn, *Am. J. Roentgenol.* **2000**, *174*, 405.
[39] J. L. Lewis, S. L. Johnson, *J. Anat.* **2001**, *199*, 483.
[40] J. Diani, B. Fayolle, P. Gilormini, *Eur. Polym. J.* **2009**, *45*, 601.
[41] S. R. Shin, H. Bae, J. M. Cha, J. Y. Mun, Y. C. Chen, H. Tekin, H. Shin, S. Farshchi, M. R. Dokmeci, S. Tang, A. Khademhosseini, *ACS Nano* **2012**, *6*, 362.
[42] D. Kai, M. P. Prabhakaran, B. Stahl, M. Eblenkamp, E. Wintermantel, S. Ramakrishna, *Nanotechnology* **2012**, *23*, 95705.
[43] A. Agrawal, N. Rahbar, P. D. Calvert, *Acta Biomater.* **2013**, *9*, 5313.
[44] I. C. Liao, F. T. Moutos, B. T. Estes, X. Zhao, F. Guilak, *Adv. Funct. Mater.* **2013**, *23*, 5833.